(13) Balta Calleja, F. J.; Hosemann, R. *J. Polym. Sci., Polym. Phys. Ed.* **1980**, *18*, 1159.
(14) Richardson, M. J.; Flory, P. J.; Jackson, J. B. *Polymer* **1963**, *4*, 221.
(15) Bunn, C. W. In *Polyethylene*; Renfrew, A.; Morgan, P., Eds.; Illife: London, 1957; Chapter 5.
(16) Alamo, R.; Domszy, R. C.; Mandelkern, L. *J. Phys. Chem.* **1984**, *88*, 6587.
(17) Keller, A.; Priest, D. J. *J. Macromol. Sci., Phys.* **1968**, *B2*, 479.
(18) Keller, A.; Priest, D. J. *J. Polym. Sci., Part B* **1970**, *8*, 13.
(19) Witenhafer, D. E.; Koenig, J. L. *J. Polym. Sci., Polym. Phys. Ed.* **1969**, *7*, 1279.
(20) Runt, J.; Harrison, I. R. *J. Polym. Sci., Polym. Phys. Ed.* **1978**, *16*, 375.
(21) Vonk, C. G.; Pijpers, A. P. *J. Polym. Sci., Polym. Phys. Ed.* **1985**, *23*, 2517.
(22) Vile, J.; Hendra, P. J.; Wilis, H. A.; Cudby, M. E. A.; Bunn, A. *Polymer* **1984**, *25*, 1173.
(23) Holdsworth, P. J.; Keller, A. *Makromol. Chem.* **1969**, *125*, 82.
(24) Domszy, R. C.; Alamo, R.; Mathieu, P. J. M.; Mandelkern, L. *J. Polym. Sci., Polym. Phys. Ed.* **1984**, *22*, 1727.
(25) Vanderhart, D. L.; Pérez, E. *Macromolecules* **1986**, *19*, 1902.
(26) Pines, A.; Gibby, M. G.; Waugh, J. S. *J. Chem. Phys.* **1973**, *59*, 569.
(27) Sarles, L. R.; Cotts, R. M. *Phys. Rev.* **1958**, *111*, 853.
(28) Andrew, E. R. *Prog. Nucl. Magn. Reson. Spectrosc.* **1972**, *8*, 1.
(29) Lowe, I. J. *Phys. Rev. Lett.* **1959**, *2*, 85.
(30) Schaefer, J.; Stejskal, E. O.; Buchdahl, R. *Macromolecules* **1975**, *8*, 291.
(31) Garroway, A. N.; Moniz, W. B.; Resing, H. A. *Coat. Plast. Prepr. Pap. Meet. (Am. Chem. Soc., Div. Org. Coat. Plast. Chem.)* **1976**, *36*, 133.
(32) Certain commerical companies are named in order to specify adequately the experimental procedure. This in no way implies endorsement or recommendation by NBS.
(33) Stejskal, E. O.; Schaefer, J. *J. Magn. Reson.* **1977**, *28*, 105.
(34) Randall, J. C. In *Polymer Characterization by ESR and NMR*; ACS Symposium Series 142; Woodward, A. E., Bovey, F. A., Eds.; American Chemical Society: Washington, DC, 1980.
(35) Rachapudy, H.; Smith, G. G.; Raju, V. R.; Graessley, W. W. *J. Polym. Sci., Polym. Phys. Ed.* **1979**, *17*, 1211.
(36) Randall, J. C. *J. Polym. Sci., Polym. Phys. Ed.* **1975**, *13*, 1975.
(37) Krigas, T. M.; Carella, J. M.; Strujlinski, M. J.; Crist, B.; Graessley, W. W.; Schilling, F. C. *J. Polym. Sci., Polym. Phys. Ed.* **1985**, *23*, 509.
(38) Crist, B.; Graessley, W. W.; Wignall, G. D. *Polymer* **1972**, *23*, 1561.
(39) Howard, P. R. Ph.D. Thesis, Northwestern University, 1986.
(40) Noggle, J. H.; Schirmer, R. E. In *The Nuclear Overhauser Effect*; Academic: New York, 1971.
(41) Torchia, D. A. *J. Magn. Reson.* **1978**, *30*, 613.
(42) Axelson, D. E.; Mandelkern, L.; Popli, R.; Mathieu, P. *J. Polym. Sci., Polym. Phys. Ed.* **1983**, *21*, 2319.
(43) Axelson, D. E. *J. Polym. Sci., Polym. Phys. Ed.* **1982**, *20*, 1427.
(44) Kitamaru, R.; Horii, F.; Murayama, K. *Macromolecules* **1986**, *19*, 636.
(45) Schröter, B.; Posern, A. *Makromol. Chem., Rapid Commun.* **1982**, *3*, 623.
(46) Axelson, D. E.; Levy, G. C.; Mandelkern, L. *Macromolecules* **1979**, *12*, 41.
(47) (a) Dorman, D. E.; Otocka, E. P.; Bovey, F. A. *Macromolecules* **1972**, *5*, 574. (b) Bovey, F. A.; Schilling, F. C.; McCrackin, F. L.; Wagner, H. L. *Macromolecules* **1976**, *9*, 76.
(48) Usami, T.; Takayama, S. *Macromolecules* **1984**, *17*, 1756.
(49) Ostroff, E. D.; Waugh, J. S. *Phys. Rev. Lett.* **1966**, *16*, 1097.
(50) Seguela, R.; Rietsch, F. *J. Polym. Sci., Polym. Lett. Ed.* **1986**, *24*, 29.
(51) Laupetre, F.; Monnerie, L.; Barthelemy, L.; Vairon, J. P.; Sauzeau, A.; Roussel, D. *Polym. Bull. (Berlin)* **1986**, *15*, 159.
(52) Guttman, C. M.; DiMarzio, E. A.; Hoffman, J. D. *Polymer* **1981**, *22*, 1466.
(53) VanderHart, D. L., to be published.
(54) VanderHart, D. L.; Khoury, F. *Polymer* **1984**, *25*, 1589.
(55) Schneider, B.; Pivocova, H.; Doskocilova, D. *Macromolecules* **1972**, *5*, 1589.
(56) Garroway, A. N.; Moniz, W. B.; Resing, H. A. *Carbon-13 NMR in Polymer Science*; ACS Symposium Series 103; W. M. Pasika, Ed.; American Chemical Society: Washington, DC, 1979.

Small-Angle Scattering of the Statistical Structure of Domain Boundaries

W. Ruland

Fachbereich Physikalische Chemie, Bereich Polymere, Universität Marburg, D-3550 Marburg/Lahn, F.R.G. *Received June 9, 1986*

ABSTRACT: The determination of the width of domain boundaries by the SAXS method can contain substantial errors if the boundary region is not represented by a smooth homogeneous density transition but by a statistical structure of a certain coarseness. It is shown that these errors lead, in general, to an underestimation of the values of the boundary widths and to a compensation of the expected increase of these values with temperature in the case of block copolymers. SAXS studies of samples with a high preferred orientation of the interface planes can be used to minimize the errors and to obtain information on the coarseness of the statistical structure of the domain boundaries.

Introduction

The width of domain boundaries is an important parameter for the characterization of microphase separation in polymers. By use of small-angle X-ray scattering, this parameter is obtained by measurements in the range of validity of Porod's law.[1-8] In this range, the correct subtraction of the background is essential for an accurate determination of the boundary width, especially in the case of slit-smeared intensities.[6]

The theory of microphase separation in block copolymers[9-11] predicts the relationship

$$d_z = 2\langle a \rangle / (6\chi)^{1/2} \quad (1)$$

where d_z is the boundary width, χ the Flory–Huggins interaction parameter, and $\langle a \rangle$ the average length of a monomer unit. Consequently, measurements of d_z as a function of temperature could, in principle, be used to determine the temperature dependence of χ.

SAXS measurements carried out by Roe, Fishkis, and Chang[5] on block copolymer melts did not, however, show the decrease of the intensity at large scattering angles predicted by the temperature dependence of d_z according to eq 1. This observation was confirmed by similar measurements carried out in my research group, the details of which will be reported in a separate paper. Furthermore, the d_z values determined for block copolymers at room temperature were found to be significantly smaller than the theoretically predicted ones.[6] The aim of this paper is to investigate the possibility of an influence of the statistical structure of the domain boundaries on the de-

0024-9297/87/2220-0087$01.50/0

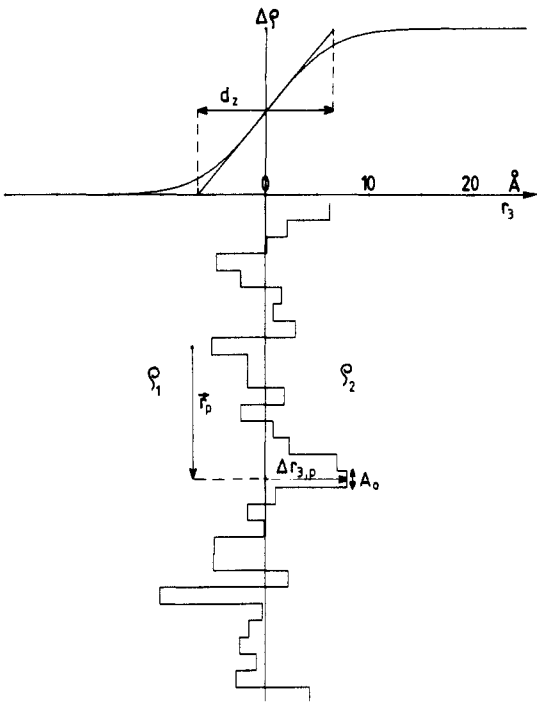

Figure 1. Schematic presentation of the statistical structure of a domain boundary and its average density profile. d_z is the domain boundary width, r_3 is the distance perpendicular to the interface plane, $\mathbf{r}_p$ and $\Delta r_{3,p}$ are the positions of the local density transitions, and A_0 is the surface of the shape function Y_0.

termination of d_z, which could explain the differences between experimental and theoretical values.

Scattering of a Statistical Boundary Structure

Figure 1 shows a scheme of a statistical density distribution at a domain boundary and its relationship to the boundary profile and to d_z. Such a structure can be approximated by

$$\Delta\rho(\mathbf{r}) = (\rho_1 - \rho_2)\sum_p Y_p{}^*\delta(\mathbf{r} - \mathbf{r}_p)$$

where $\Delta\rho$ is the electron density distribution, ρ_1 and ρ_2 are the electron densities of phases 1 and 2, respectively, and δ is the Dirac δ distribution. The vectors, $\mathbf{r}_p$, which are oriented parallel to the plane of the interface, define a two-dimensional point distribution of short-range order. The function Y_p describes the local details of the boundary structure (see Figure 1)

$$Y_p(\mathbf{r}) = Y_0(\mathbf{r}_{12})\ \mathrm{sgn}\ (r_3 - \Delta r_{3,p})/2$$

where sgn is the sign function, Y_0 is a shape function defining the coarseness of the interface structure, $\mathbf{r}$ is the position vector with the components $\mathbf{r}_{12} = (r_1, r_2)$ parallel and r_3 perpendicular, respectively, to an ideally plane interface and $\Delta r_{3,p}$ is the local deviation perpendicular to this plane as a function of $\mathbf{r}_p$. The asterisk stands for three-dimensional convolution. Using the relationship

$$I(\mathbf{s}) = |\mathfrak{F}(\Delta\rho(\mathbf{r}))|^2$$

where I is the scattering intensity, $\mathfrak{F}$ stands for three-dimensional Fourier transform, and $\mathbf{s}$ is the vector in reciprocal space ($s = 2\sin\theta/\lambda$), one finds, in analogy to the treatment of substitutional disorder in lattices[12]

$$I(\mathbf{s}) = (\rho_1 - \rho_2)^2[n(\langle|\Phi|^2\rangle - |\langle\Phi\rangle|^2) + |\langle\Phi\rangle|^2|Z|^2] \quad (2)$$

provided that no correlation exists between the local deviations $\Delta r_{3,p}$ and the vectors $\mathbf{r}_p$.

The function $\Phi_p(\mathbf{s})$ is the Fourier transform of $Y_p(\mathbf{r})$

$$\Phi_p(\mathbf{s}) = \Phi_0(\mathbf{s}_{12})\ i\ \exp(2\pi i\Delta r_{3,p}s_3)/(2\pi s_3)$$

where $\mathbf{s}_{12}$ and s_3 are the components of the vector $\mathbf{s}$ parallel and perpendicular, respectively, to the interface plane and Φ_0 is the Fourier transform of Y_0.

The average $\langle\Phi\rangle$ is taken over all lattice sites, and n is the total number of sites. This leads to

$$\langle\Phi\rangle(\mathbf{s}) = \Phi_0(\mathbf{s}_{12})\ i\langle\exp(2\pi i\Delta r_{3,p}s_3)\rangle/(2\pi s_3)$$

The average on the right-hand side of this equation is given by

$$\langle\exp(2\pi i\Delta r_{3,p})\rangle = \int_{-\infty}^{\infty} h(\Delta r_3)\exp(2\pi i\Delta r_3 s_3)\,\mathrm{d}\Delta r_3 = H(s_3)$$

where $h(\Delta r_3)$ is the probability density of Δr_3 and $H(s_3)$ its Fourier transform. These two functions are identical with those already defined in the earlier papers.[1,6] If h is taken to be Gaussian, H is represented by

$$H(s_3) = \exp[-\pi(d_z s_3)^2]$$

If the density profile is taken to be a tanh function,[9-11] h is given by

$$h(\Delta r_3) = \mathrm{sech}^2\,(2\Delta r_3/d_z)/d_z$$

Consequently

$$H(s_3) = \pi^2 d_z s_3\ \mathrm{csch}\ (\pi^2 d_z s_3/2)/2$$

In both cases, d_z is defined as the integral width of h. Its relationship to the variance $\sigma_z{}^2$ of h is

$$d_z = (2\pi)^{1/2}\sigma_z$$

for a Gaussian and

$$d_z = 4(3^{1/2})\sigma_z/\pi$$

for sech.[2]

Equation 2 indicates that the scattering intensity is the sum of two components

$$I = I_z + I_S$$

where

$$I_z = (\rho_1 - \rho_2)^2 n(\langle|\Phi|^2\rangle - |\langle\Phi\rangle|^2)$$

$$I_S = (\rho_1 - \rho_2)^2|\langle\Phi\rangle|^2|Z|^2$$

We consider first the component I_S. The function $|Z|^2$ is given by

$$|Z|^2 = |\mathfrak{F}[\sum_p \delta(\mathbf{r} - \mathbf{r}_p)]|^2$$

Assuming that the short-range order is based on first-neighbor distances in the range of the side-by-side packing distances of chain segments, the predominant contribution of $|Z|^2$ to the small-angle scattering is given by

$$|Z|^2 \simeq |\Phi_S(\mathbf{s}_{12})|^2/A_0{}^2$$

where Φ_S is the Fourier transform of the shape function of the total interface S and A_0 is the area of the cross section of the shape function Y_p parallel to the interface plane. Since S is, in general, very large compared to A_0, $|Z|^2$ can be approximated by

$$|Z|^2 \simeq S\delta(\mathbf{s}_{12})/A_0{}^2$$

for s_{12} larger than $S^{1/2}$, and one obtains

$$I_S(\mathbf{s}) = (\rho_1 - \rho_2)^2 S H^2(s_3)\delta(\mathbf{s}_{12})/(2\pi s_3)^2 \quad (3)$$

since $|\Phi_0|^2(0) = A_0{}^2$.

Averaging I_S over all directions in reciprocal space (solid angle ω) results in

$$I_S = \langle I_S \rangle_\omega = (\rho_1 - \rho_2)^2 S H^2(s)/(8\pi^3 s^4)$$

which is Porod's law corrected for finite boundary width.

This expression is equivalent to that already derived in the earlier paper.[1] It is representative for the scattering of a two-phase structure with a smooth boundary profile of finite width

$$I_S = I_{id} H^2$$

where I_{id} is the scattering of the same two-phase structure with infinitely sharp boundaries.

The component I_z represents the scattering due to the local fluctuation of the concentration of phase 1 and phase 2 within the domain boundary. Since

$$|\Phi_p|^2 = |\Phi_0(\mathbf{s}_{12})|^2/(2\pi s_3)^2 = \langle |\Phi|^2 \rangle$$

and $n \simeq S/A_0$, one obtains

$$I_z(\mathbf{s}) = (\rho_1 - \rho_2)^2 S |\Phi_0(\mathbf{s}_{12})|^2 [1 - H^2(s_3)]/[A_0(2\pi s_3)^2] \quad (4)$$

Random Orientation

For a comparison of I_z and I_S we consider first a two-phase structure with a random orientation of the interface boundary. This leads to

$$I_z = \langle I_z \rangle_\omega = (\rho_1 - \rho_2)^2 S \langle |\Phi_0(\mathbf{s}_{12})|^2 [1 - H^2(s_3)]/[A_0(2\pi s_3)^2] \rangle_\omega$$

where $\langle\ \rangle_\omega$ stands for averaging over the solid angle ω. To simplify the calculations we assume Φ_0 to be a radially symmetrical Gaussian distribution

$$|\Phi_0|^2 \simeq A_0^2 \exp[-(\pi R_0 s_{12})^2]$$

where $A_0 = \pi R_0^2$, and furthermore

$$H(s_3) \simeq \exp[-2(\pi \sigma_z s_3)^2]$$

When polar coordinates $s_{12} = s \sin \phi$ and $s_3 = s \cos \phi$ are used, the spherical averaging leads to the expression

$$I_z(s) = (\rho_1 - \rho_2)^2 S A_0 \sigma_z^2 G_\omega(s)$$

where

$$G_\omega(s) = \exp(-a) \int_0^1 (1/bz^2) \exp(az^2)[1 - \exp(-bz^2)]\, dz$$

with $a = (\pi R_0 s)^2$, $b = (2\pi \sigma_z s)^2$, and $z = \cos \phi$.

The integral results in

$$G_\omega = \{\exp(-b) - 1 + 2 \exp(-a) \times [a^{1/2}\ \mathrm{Erfi}\ (a^{1/2}) + (b - a)^{1/2}\ \mathrm{Erf}\ ((b - a)^{1/2})]\}/b$$

where

$$\mathrm{Erf}\ (x) = \int_0^x \exp(-t^2)\, dt$$

$$\mathrm{Erfi}\ (x) = \int_0^x \exp(t^2)\, dt$$

For small values of s, G_ω is approximated by

$$G_\omega \simeq 1 - 2\pi^2 s^2 (R_0^2 + \sigma_z^2)/3$$

i.e., the radius of gyration is

$$R_G^2 = (R_0^2 + \sigma_z^2)/2$$

Figure 2 shows plots of G_ω vs. $\sigma_z s$ for various ratios R_0/σ_z. In order to assess the influence of I_z on the determination of d_z, we consider a lamellar two-phase system with I_{id} given by

$$I_{id} = S(\rho_1 - \rho_2)^2\ \mathrm{Re}\ [(1 - H_1)(1 - H_2)/(1 - H_1 H_2)]/(8\pi^3 s^4)$$

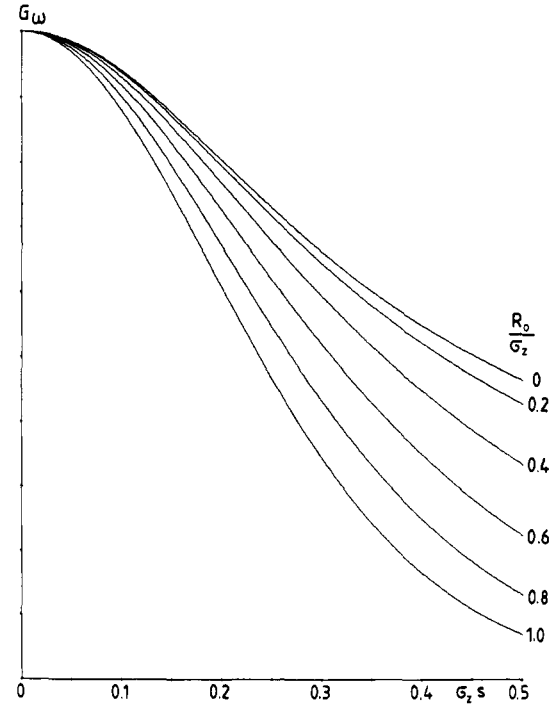

Figure 2. SAXS of the statistical structure of a domain boundary, scattering function G_ω of the spherical average calculated for various ratios R_0/σ_z plotted vs. $\sigma_z s$.

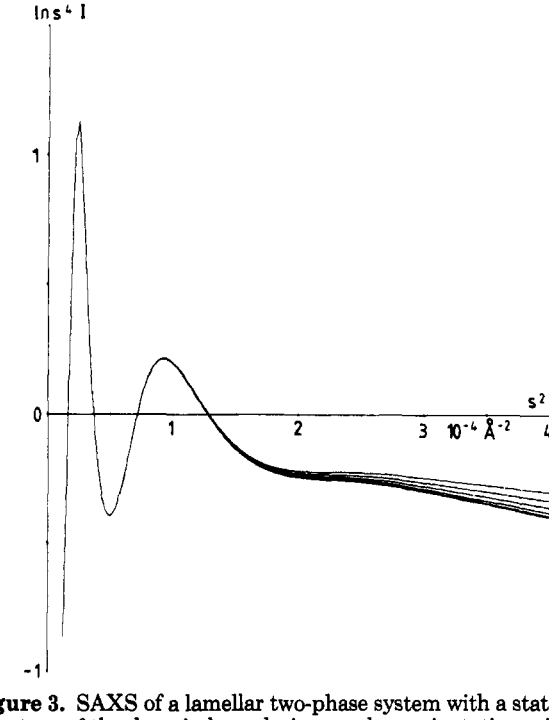

Figure 3. SAXS of a lamellar two-phase system with a statistical structure of the domain boundaries, random orientation, pinhole collimation, $\sigma_z = 5$ Å, and R_0 from 0 (lower curve) to 5 Å (upper curve) in steps of 1 Å.

where the real part Re of the expression in square brackets corresponds to the interference function of a one-dimensional short-range order[13] in the lamellar stacking. H_1 and H_2 are the Fourier transforms of the thickness distributions of the lamellae of phases 1 and 2, respectively.

Pinhole Collimation. Figures 3–5 show theoretical SAXS curves in the appropriate plots for pinhole collimation, ln $s^4 I(s)$ vs. s^2, for a lamellar system with the average period $L = 200$ Å, volume concentration $c_1 = 0.3$, and a statistical variation of the thicknesses of the lamellae

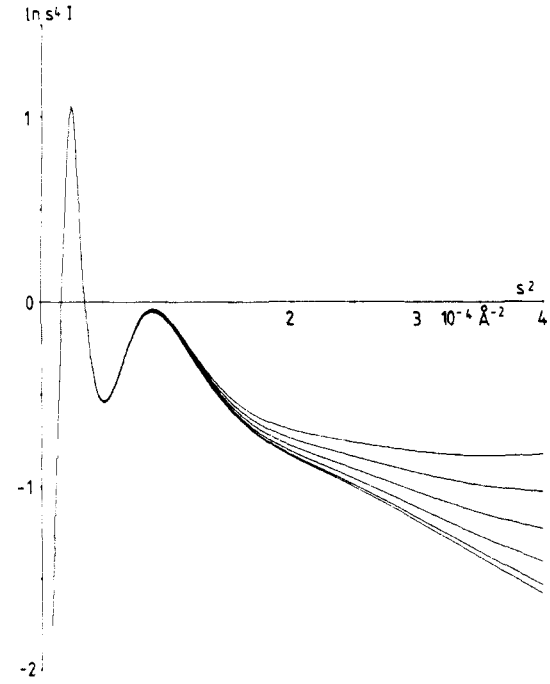

Figure 4. SAXS of a lamellar two-phase system with a statistical structure of the domain boundaries, random orientation, pinhole collimation, σ_z = 10 Å, and R_0 from 0 (lower curve) to 5 Å (upper curve) in steps of 1 Å.

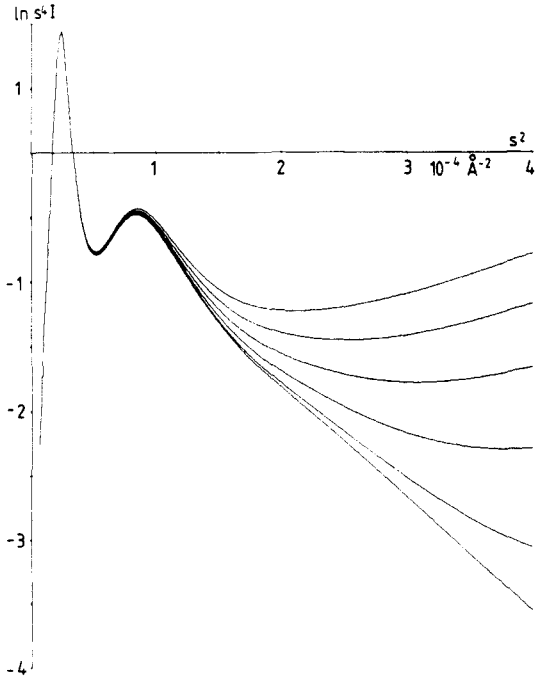

Figure 5. SAXS of a lamellar two-phase system with a statistical structure of the domain boundaries, random orientation, pinhole collimation, σ_z = 15 Å, and R_0 from 0 (lower curve) to 5 Å (upper curve) in steps of 1 Å.

large enough to suppress the interference maxima of higher order. σ_z values were chosen to correspond approximately to the theoretical values for styrene–butadiene block copolymers in the temperature range 25–300 °C. R_0 is varied from 0 to 5 Å. The curves are normalized such that

$$\lim_{s\to\infty} s^4 I_{id} = 1$$

An inspection of these curves shows clearly that the statistical structure of the domain boundaries causes systematic deviations from the expected linear relationship

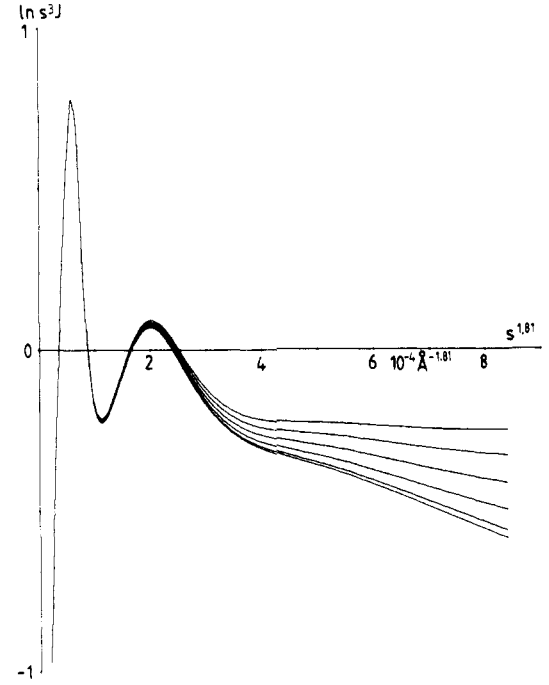

Figure 6. SAXS of a lamellar two-phase system with a statistical structure of the domain boundaries, random orientation, slit smearing, σ_z = 5 Å, and R_0 from 0 (lower curve) to 5 Å (upper curve) in steps of 1 Å.

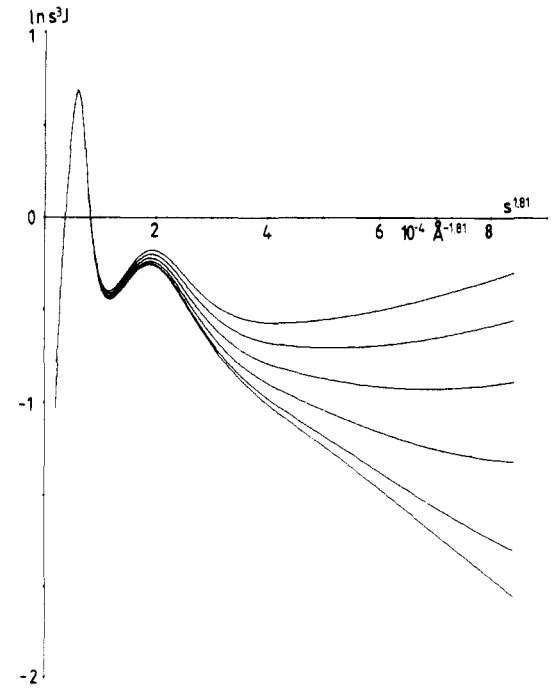

Figure 7. SAXS of a lamellar two-phase system with a statistical structure of the domain boundaries, random orientation, slit smearing σ_z = 10 Å, and R_0 from 0 (lower curve) to 5 Å (upper curve) in steps of 1 Å.

in the ln s^4I vs. s^2 plots and that these deviations tend to compensate the effect of increasing σ_z.

Slit Collimation. SAXS curves are very often measured with a slit collimation (e.g., Kratky camera), which results in "smeared" intensity distributions. Since I_S is decreasing more steeply with s than is I_z, the effect of I_z on the determination of d_z is expected to be enhanced by slit smearing. This is shown in Figures 6–8 where the slit-smeared intensities $J(s)$ corresponding to those used for the calculation of the curves in Figures 3–5 are shown

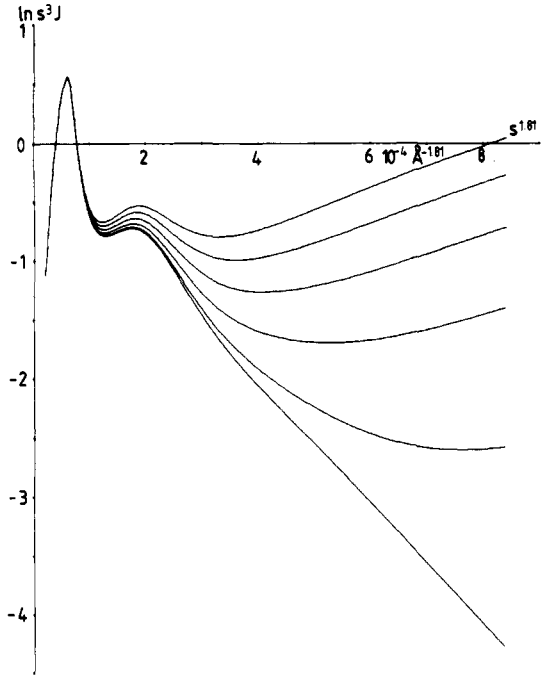

Figure 8. SAXS of a lamellar two-phase system with a statistical structure of the domain boundaries, random orientation, slit smearing σ_z = 15 Å, and R_0 from 0 (lower curve) to 5 Å (upper curve) in steps of 1 Å.

in ln s^3J vs. $s^{1.81}$ plots. The functions $J(s)$ are calculated by using the integral

$$J(s) = 2\int_0^\infty I[(s^2 + y^2)^{1/2}]W(y)\,dy$$

For $W(y)$, the slit transmission function, experimental values for standard Kratky cameras were used. The exponent 1.81 has been proposed by Koberstein, Morra, and Stein[4] as an approximation for the effect of slit smearing on the function H^2 in the range of validity of Porod's law. The curves show the expected increase of the influence of the statistical structure of the domain boundaries on the determination of d_z as a result of slit smearing.

Preferred Orientation

Special methods of sample preparation result in a preferred orientation of lamellar or cylindrical two-phase systems.[8,14,15] Such samples improve, in general, the interpretation of SAXS curves and the accuracy of the determination of structural parameters. For lamellar two-phase systems, the most favorable case is an arrangement of the lamellae parallel to a given plane of the sample, i.e., a preferred orientation of the perpendiculars of the lamellae in the direction of the principal axis of a system of cylindrical symmetry.

We consider such a lamellar system in which the orientation of the perpendiculars is defined by the distribution $g(\phi)$, where ϕ is the angle between a perpendicular and the principal axis. For perfect orientation, I_S and I_z are given by eq 3 and 4, respectively. Since I_S and I_z are cylindrically symmetrical about the s_3 direction, we can use polar coordinates (s,ϕ') to define **s**.

The intensity distribution for a given $g(\phi)$ is obtained by the integral transformation[16]

$$I(s,\phi) = \int_0^{\pi/2} I_0(s,\phi')F(\phi,\phi')\sin\phi'\,d\phi'$$

where I_0 is the intensity distribution for perfect orientation

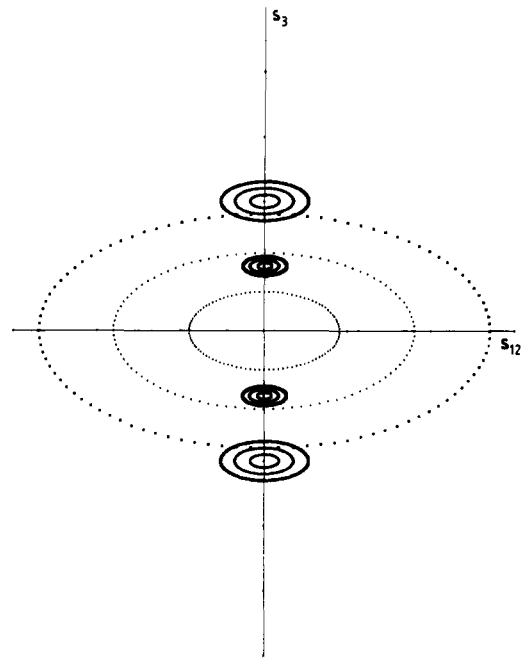

Figure 9. Schematic presentation of the two-dimensional SAXS intensity distribution for a lamellar two-phase system with preferred orientation and statistical structure of the domain boundaries.

and the kernel $F(\phi,\phi')$ can be calculated from $g(\phi)$.[17]

For I_S, this transformation results in

$$I_S(s,\phi) = (\rho_1 - \rho_2)^2 S H^2(s) g(\phi)/(8\pi^3 s^4)$$

if $g(\phi)$ is normalized such that

$$\int_0^{\pi/2} g(\phi)\sin\phi\,d\phi = 1$$

For I_z, the result of the transformation is more complicated in the general case. One can, however, show that $I_z(s,\phi{=}0)$ can be approximated by

$$I_z(s,0) = (\rho_1 - \rho_2)^2 S A_0[1 - H^2(s)]/[(2\pi s)^2(1 + \pi(R_0 B_\phi s)^2)]$$

if B_ϕ, the integral width of $g(\phi)$, is small.

Figure 9 shows a schematic presentation of the intensity distribution in a section in reciprocal space containing the principal axis of orientation s_3. The interference maxima centered on the s_3 axis represent the maxima in I_S. Their broadening perpendicular to the s_3 axis is due to the orientation distribution $g(\phi)$. The broad intensity distribution centered on the origin of reciprocal space represents I_z. An inspection of this intensity distribution shows that, in measurements with a pinhole collimation along the s_3 direction, the contribution of I_S is predominant, whereas measurements along the s_{12} direction are, except for very small angles, only determined by I_z. In fact, a Guinier plot of the intensity measured along s_{12} should lead to the determination of R_0.

Figures 10 and 11 show plots of ln $s^4I(s,0)$ vs. s^2 for a σ_z value of 15 Å, R_0 values ranging from 0 to 5 Å, and B_ϕ values of 20° and 40°. The curves show clearly that the contribution of I_z is considerably reduced and the error in the determination of d_z is small.

Calculations of SAXS curves obtainable by measurements in the s_3 direction with a slit system oriented parallel to s_{12} are shown in Figures 12 and 13 for the same structural parameters as those used in Figures 10 and 11. In this case, the appropriate plot is ln s^3 vs. s^2. These curves demonstrate that the effect of slit smearing is much less pronounced for samples with sufficiently high preferred

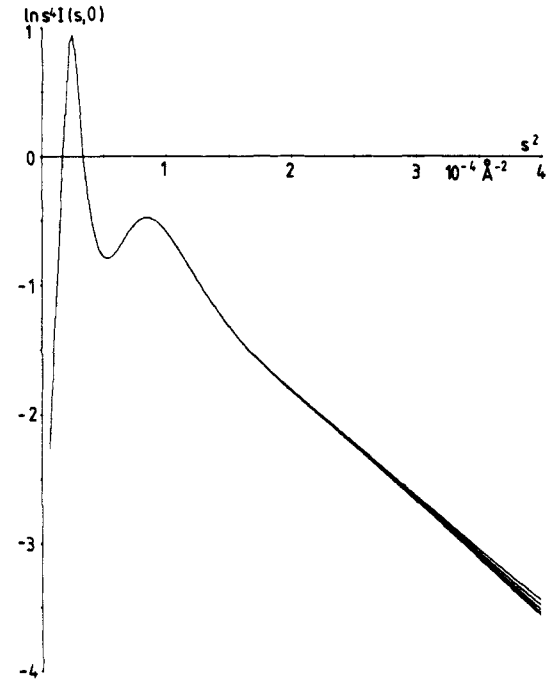

Figure 10. SAXS of a lamellar two-phase system with a statistical structure of the domain boundaries, preferred orientation, orientation half-width 20, pinhole collimation, measurement along principal axis of orientation, σ_z = 15 Å, and R_0 from 0 (lower curve) to 5 Å (upper curve) in steps of 1 Å.

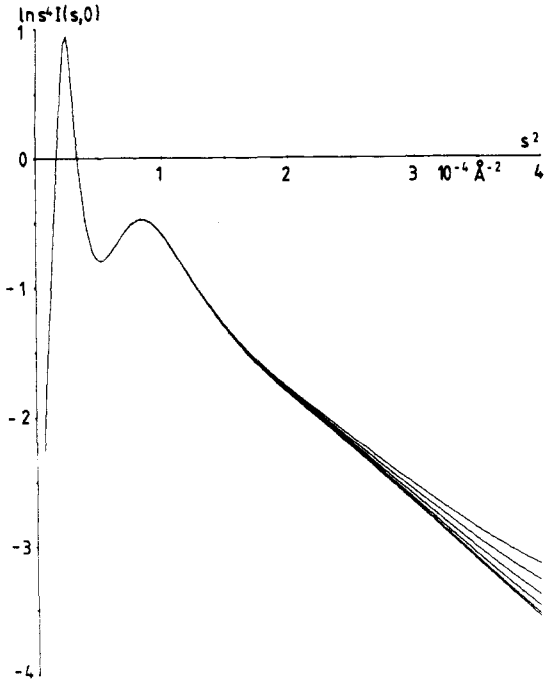

Figure 11. SAXS of a lamellar two-phase system with a statistical structure of the domain boundaries, preferred orientation, orientation half-width 40, pinhole collimation, measurement along principal axis of orientation, σ_z = 15 Å, and R_0 from 0 (lower curve) to 5 Å (upper curve) in steps of 1 Å.

orientation than for samples with random orientation, but the errors in the determination of d_z are still appreciable.

Conclusions

If the finite width of domain boundaries is due to a statistical structure of the boundaries instead of a smooth homogeneous density transition, the determination of the boundary width by SAXS methods can contain substantial errors. These errors are minimized by the study of samples with high preferred orientation of the interface planes.

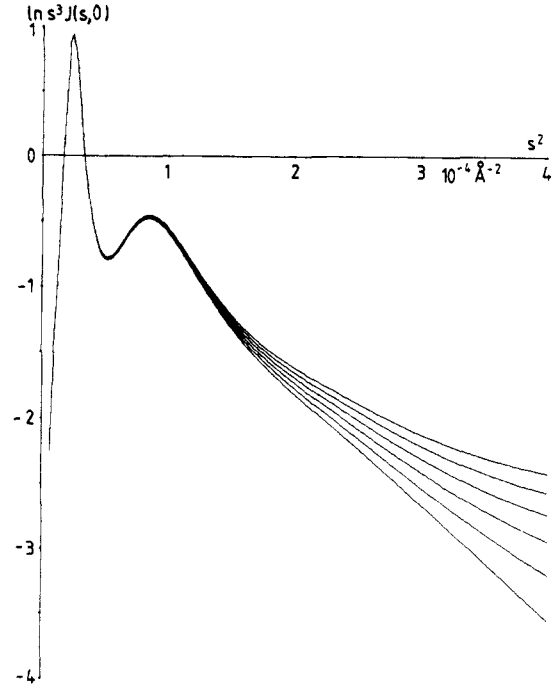

Figure 12. SAXS of a lamellar two-phase system with a statistical structure of the domain boundaries, preferred orientation, orientation half-width 20, slit smearing, measurement along principal axis of orientation, σ_z = 15 Å, and R_0 from 0 (lower curve) to 5 Å (upper curve) in steps of 1 Å.

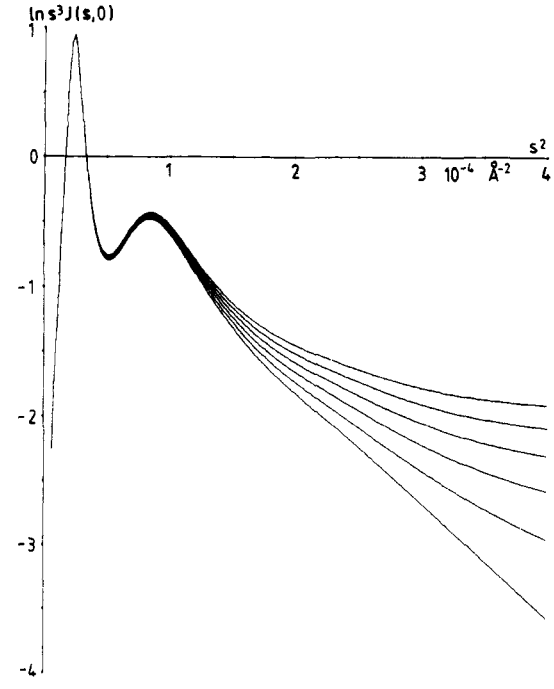

Figure 13. SAXS of a lamellar two-phase system with a statistical structure of the domain boundaries, preferred orientation, orientation half-width 40, slit smearing, measurement along principal axis of orientation, σ_z = 15 Å, and R_0 from 0 (lower curve) to 5 Å (upper curve) in steps of 1 Å.

Direction-dependent intensity measurements of such samples can be used to obtain information on the coarseness of the boundary structure.

The structural model used for the calculations limits the applicability of the results to boundary widths corresponding to the lengths of a few Kuhn segments. For larger boundary widths, the flexibility of the chains has to be taken into account, and a more involved model for the fluctuation of the segment density in the boundary

region has to be developed. This is expected to lead to somewhat different values for the additional intensity component I_z but will not change the general effect of this component on the SAXS curves.

Acknowledgment. I am indebted to Dr. A. R. Khokhlov for useful discussions.

References and Notes

(1) Ruland, W. *J. Appl. Crystallogr.* **1971**, *4*, 70.
(2) Vonk, C. G. *J. Appl. Crystallogr.* **1973**, *6*, 81.
(3) Todo, A.; Hashimoto, T.; Kawai, H. *J. Appl. Crystallogr.* **1978**, *11*, 558.
(4) Koberstein, J. T.; Morra, B.; Stein, R. S. *J. Appl. Crystallogr.* **1980**, *13*, 34.
(5) Roe, R.-J.; Fishkis, M.; Chang, J. C. *Macromolecules* **1980**, *14*, 1091.
(6) Siemann, U.; Ruland, W. *Colloid Polym. Sci.* **1982**, *260*, 999.
(7) Zin, W.-C.; Roe, R.-J. *Macromolecules* **1984**, *17*, 183.
(8) Annighöfer, F.; Gronski, W. *Makromol. Chem.* **1984**, *185*, 2213.
(9) Helfand, E.; Tagami, Y. *Polym. Lett.* **1971**, *9*, 741.
(10) Helfand, E.; Tagami, Y. *J. Chem. Phys.* **1972**, *56*, 3592.
(11) Semenov, A. N. *Zh. Eksp. Teor. Fiz.* **1985**, *88*, 1242.
(12) See, e.g.: Guinier, A. *Théorie et Technique de la Radiocristallographie*, 3rd ed.; Dunod: Paris, Chapter 13.6.
(13) Hermans, J. J. *Recl. Trav. Chim. Pays-Bas* **1944**, *63*, 5.
(14) Hadziioannou, G.; Mathis, A.; Skoulios, A. *Colloid Polym. Sci.* **1979**, *257*, 15.
(15) Hadziioannou, G.; Skoulios, A. *Macromolecules* **1982**, *15*, 258.
(16) Ruland, W. *Colloid Polym. Sci.* **1977**, *255*, 833.
(17) Ruland, W.; Tompa, H. *Acta Crystallogr., Sect. A: Cryst. Phys., Diffr., Theor. Gen. Crystallogr.* **1968**, *A24*, 93.

Light Scattering Characterization of an Alternating Copolymer of Ethylene and Tetrafluoroethylene. 1. Static and Dynamic Properties

Benjamin Chu* and Chi Wu

Chemistry Department, State University of New York at Stony Brook, Long Island, New York 11794. *Received April 17, 1986*

ABSTRACT: Laser light scattering, including the angular dependence of the absolute integrated scattered intensity and its spectral distribution, has been used successfully to characterize, for the first time, an alternating copolymer of ethylene and tetrafluoroethylene, $-(CH_2CH_2CF_2CF_2)_x-$, in diisobutyl adipate at 240 °C. In order to carry out experiments at high temperatures, we developed a new filtration apparatus and a new light scattering spectrometer capable of refractive index increment measurements. The results show that over the molecular weight range 5×10^5 to 1.2×10^6, our copolymer samples obey the scaling relations $\langle R_g^2 \rangle_z^{1/2} = 1.68 \times 10^{-1} M_w^{0.60}$ and $D_0° = 3.35 \times 10^{-4} M_w^{-0.60}$, with $\langle R_g^2 \rangle_z^{1/2}$, M_w, and $D_0°$ being the z-average root-mean-square radius of gyration (Å), the weight-average molecular weight, and the translational diffusion coefficient at infinite dilution (cm^2/s), respectively. Furthermore, the variance ($\mu_2/\bar{\Gamma}^2$) of the photoelectron count time correlation function shows a small value (~0.1), suggesting surprisingly narrow molecualr weight distributions for our copolymer samples.

I. Introduction

Laser light scattering (LLS) has been used to characterize a variety of polymers, including poly(1,4-phenylene terephthalamide) (PPTA)[1-5] and polyethylenes (PE).[6,7] The advantages of LLS are numerous. It is noninvasive. It has a wide dynamic range covering sizes from tens of angstroms to microns. The technique also permits determination of polydispersity in terms of molecular weight distributions, especially for unimodal functions of arbitrary shapes, without an a priori assumption on the form of the distribution function. In particular, LLS has been effective in characterizing polymer solutions at high temperatures,[6,7] e.g., at more than 200 °C for poly(dichlorophosphazene) in hexachlorotriphosphazene[8]), and polyelectrolytes (PPTA) in concentrated sulfuric acid, with and without added salt.[1-5] Thus, a natural extension and challenge in the application of LLS to polymer solution characterization is to examine static and dynamic properties of fluorocarbon polymers that defy characterization, simply because they are essentially insoluble in any ordinary solvents. Although our ultimate aim is to characterize poly(tetrafluoroethylene), $-(CF_2CF_2)_x-$, commercially known as Teflon (a registered trademark of Du Pont), we have to approach the characterization of poly(tetrafluoroethylene) (PTFE) slightly differently in view of the structural complexities associated with the solvent and plan to report our findings on PTFE later. In this (1) and a subsequent article (2), we report details of the characterization of a Teflon copolymer, an alternating copolymer of ethylene and tetrafluoroethylene (PETFE), $-(CF_2CF_2CH_2CH_2)_y-$. An outline of our procedures has already appeared in a preliminary publication.[9] Our report on the PETFE characterization can be divided into two parts. In this article (1), we shall be concerned with experiments on static and dynamic properties of PETFE in diisobutyl adipate at 240 °C, including a description of our new high-temperature light scattering spectrometer, adaptation for use as a high-temperature differential refractometer, and the development of a new high-temperature filtration apparatus for polymer solution clarification. In the subsequent article (2), we shall consider the determination of the molecular weight distribution (MWD) of PETFE from precise time correlation function measurements using experimentally determined scaling relations between the translational diffusion coefficient and the molecular weight and three different algorithms for the Laplace inversion. We report the details of our analysis in a separate article (2) because MWD can be determined only by means of LLS. At the present time, there is no other known technique that can provide an absolute determination of MWD of PETFE.

II. Experimental Methods

1. Materials. Diisobutyl adipate was obtained from Hatco Industries and was purified by passage through a column of activated silica gel to remove acidic and basic impurities. The resulting material was 99.5% pure by vapor phase chromatography. The polymers (courtesy of W. Buck, Polymer Products

0024-9297/87/2220-0093$01.50/0